Three-Dimensional Scattering Centers Extraction of Radar Targets Using High Resolution Techniques

Jun Zhang[1, *], Jiemin Hu[1], Yangzhao Gao[2], Ronghui Zhan[1], and Qinglin Zhai[2]

Abstract—In optical region, the scattering center model is very useful in scattering analysis, target recognition and data compression. The method based on Hough transformation performs well in most cases. However, the algorithm extracts the scattering centers one by one via a clean method, which is time consuming. To solve this problem, a novel method is proposed in this paper to extract the scattering centers. By searching the estimated 1D scattering centers, the candidate positions for 3D scattering centers are extracted. Then the candidates are discriminated by a clustering based procedure. By employing the new algorithm, the 3D scattering centers can be extracted simply and the clean step is unnecessary, which makes the procedure efficient. The experiment results of the high-frequency-electromagnetic data demonstrate the performance of the proposed method.

1. INTRODUCTION

In high frequency scattering region, the response of an extended target is well approximated as a sum of responses from a discrete set of points on the target, called scattering centers [1–7]. The scattering center model provides a concise and physically relevant description of the target radar signature, which can be used in numerous radar applications. For example, using the strength and position of the scattering centers, the target echoes at different aspects, the range profiles and the SAR/ISAR images can be easily reconstructed in real time.

In order to simulate the target echoes efficiently and effectively, the global scattering center model is proposed, which is valid over a large angular extent [8, 9]. Generally, there are two approaches for global scattering center extraction: Shooting and Bouncing Ray (SBR) based technique [8] and Hough transform based technique [9]. In the first approach, the global scattering center model is obtained by combining many local 3D scattering center models at different viewing angles, which are extracted from a 3D radar image produces by SBR technique. However, each 3D imaging requires a synchronized azimuth-by-elevation aperture with a very large data amount, which makes the method infeasible. In the second approach, the scattering center model is built by repetitiously seeking the highest valued cell in parameter space, which is obtained by applying the Hough transform to the OTSM map. There is no 2-D or 3-D imaging steps in model building, so the original data amount is not very demanding. However, the parameter space needs updating after the scattering center correspond to the highest valued cell is extracted, which is terribly time consuming.

In this paper, a method to extract the global scattering center model is proposed. The global scattering center model is a 3D model which is extracted from the 1D scattering centers. The approach does not make use of the Hough transform and does not require extracting the scattering center one by one. It works under the following assumptions:

1. The locations of scattering centers are constant at different aspect angles.

---

* Corresponding author: Jiemin Hu (hujiemindawang@126.com).
[1] ATR Laboratory, National University of Defense Technology (NUDT), Changsha, China. [2] Electrical Engineering Department, National University of Defense Technology (NUDT), Changsha, China.

2. The scattering coefficients of scattering centers varies with aspect angle.

3. The type parameter, which describes the scatterer's local geometry according to the GTD theory, is not considered in this work. The reason is that the type parameter is very difficult to correctly identify unless the signal-to-noise (SNR) is sufficiently high [10]. Furthermore, its effect on the reconstructed scattering data is not notable at high frequencies where the relative bandwidth is not very large.

It should be noted that there are unstable scattering phenomena [11], for example, the back scattering of a cavity, backscattering caused by creeping or traveling waves, and micro-Doppler phenomenon caused by kinetic parts of the target. Fortunately, these unstable scattering phenomena only contribute a tiny part of the target echoes. Therefore, these scatterers will not be further discussed in this paper.

We propose a novel method to extract the global scattering centers. In this method, we first estimate the parameters of 1D scattering centers at different aspects, i.e., the 1D projective location and the scattering coefficients. After that, the candidates for 3D scattering centers are obtained by searching the estimated 1D scattering centers. Then the candidates are evaluated by associating with the estimated 1D scattering centers at different aspects and the 3D position of scattering centers are extracted using a clustering based method. Finally, the scattering coefficients at different aspects are estimated via a linear least squares algorithm. The proposed method is compared with the Hough transform based approach, where the scattering centers are extracted one by one.

This paper is organized as follows: Section 2 describes the mathematical formulation of a returned signal at different aspects. In Section 3, the novel method to extract the global scattering centers is investigated in detail. In Section 4, the performance of the proposed approach is characterized and compared with the approach described in [9], and some conclusion are drawn in the last section.

2. PROBLEM FORMULATION

The target coordinate system is depicted in Figure 1. It is well known that the electromagnetic field scattered from a target can be approximated as from a discrete set of scattering centers on the target, which can be expressed as

$$E(f, \theta, \gamma) = \sum_{k=1}^{K} a_k(\theta, \gamma) \exp\left[-j4\pi f\left(x_k \cos\gamma\cos\theta + y_k \cos\gamma\sin\theta + z_k \sin\gamma\right)/c\right]. \tag{1}$$

where c is the speed of light, f the frequency, θ the azimuth angle, and γ the elevation angle. In (1), K is the number of scattering centers. $\{x_k, y_k, z_k\}$ denotes the position of kth scattering center. At a aspect angle of (θ, γ), the projective position of kth scattering center can be calculated as
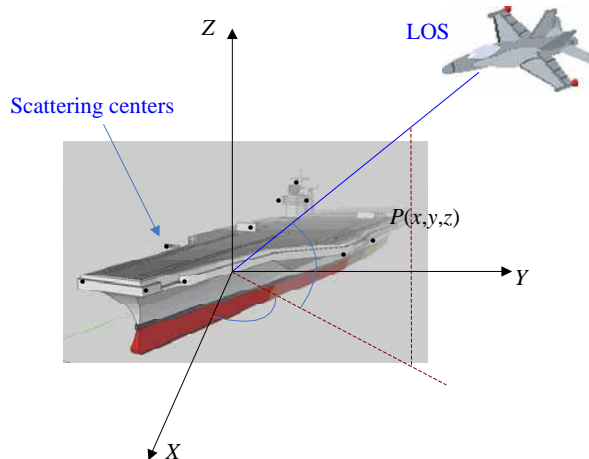
Figure 1. Geometry of scattering centers in the target coordinate system.

$r_k(\theta, \gamma) = x_k \cos\gamma\cos\theta + y_k \cos\gamma\sin\theta + z_k \sin\gamma$. $a_k(\theta, \gamma)$ represents the scattering coefficient of kth scattering center. It should be noted that $a_k(\theta, \gamma)$ varies with aspect angle (θ, γ), which means that $a_k(\theta, \gamma)$ is a function of the aspect angles (θ, γ).

The global scattering center model can be represented as

$$\mathbf{U} = \{\mathbf{A}_k, x_k, y_k, z_k\} \quad k = 1, \ldots, K \tag{2}$$

where $\mathbf{A}_k$ is an $N \times M$ complex matrix storing the scattering coefficients of the kth scattering center, i.e., the element $a_{k,n,m}$ in the nth row and mth column denotes the scattering coefficient at azimuth θ_n and elevation γ_m. N and M represent the numbers of azimuth and elevation grid points. It should be noted that the scattering coefficients not at the discrete points can be interpolated from the adjacent grid points. The global scattering center model is very useful in many radar applications [12–19] as it has some good characters: 1) the global scattering center model is not particular to radar system parameters such as operating frequency, bandwidth, and waveform; 2) the target echoes can be simulated instantly based on the model, which means that the range profiles and the SAR/ISAR images can be easily reconstructed in real time; 3) the global scattering center model has explicit physical interpretation, so it can incorporate with other information. For example, when the target configuration is changed, the corresponding scattering centers can be modified to reflect the change without rebuilding a new model.

The aim of this paper is to extract the global scattering center model $\mathbf{U}$ from the wideband measurements $E(f, \theta, \gamma)$. Generally, there are two approaches to obtain $\mathbf{U}$: the first approach extracts many local 3D scattering center models and combines them to form a global scattering center model. The disadvantage of this method is that it requires a very large data amount, which makes the method infeasible. The second approach estimates 1-D scattering centers at each viewing angle and then estimates the scatterer's 3-D position and scattering coefficients from the 1-D scattering centers. In this method, the Nyquist sampling rate is unnecessary in the azimuth and elevation dimensions. In this paper, we propose a novel method to extract the global scattering center model based on the second approach.

3. GLOBAL SCATTERING CENTERS EXTRACTION ALGORITHM

First of all, we should estimate the 1-D scattering center parameters, i.e., $r_i(\theta_n, \gamma_m)$ and $a_i(\theta_n, \gamma_m)$, from $E(f, \theta_n, \gamma_m)$, where θ_n and γ_m represent the nth sampling point in azimuth dimension and the mth sampling point in elevation dimension, respectively. $i = 1, 2, \ldots, I$, where I is the estimated number of scattering centers at aspect angle (θ_n, γ_m). Up to now, 1-D scattering centers extraction is a well studied subject and many supper-resolution algorithms are proposed, such as the structure total least norm (STLN) algorithm [20], the matrix pencil (MP) Method [21], the multiple signal classification (MUSIC) algorithm [22], estimation of signal parameters via rotational invariance techniques (ESPRIT) [23], and compressed sensing (CS) based algorithm [24]. Generally, most of them have good performances. Therefore, this paper focuses on extracting the 3D scattering centers model $\mathbf{U}$ from $r_k(\theta_n, \gamma_m)$ and $E(f, \theta_n, \gamma_m)$, where $r_k(\theta_n, \gamma_m)$ represents the projective position of kth scattering center. Herein, we realize this purpose by taking two steps: extracting the candidate positions for 3D scattering centers and candidates discriminating. This section is organized as follows. First, the details of the proposed method will be discussed. Then, the performance of the new method will be analyzed.

3.1. Algorithm

3.1.1. Extracting the Candidate Positions for 3D Scattering Centers

The candidate positions for 3D scattering centers can be obtained by applying the following steps:

1. Discrete the 3D position space $\{x, y, z\}$ within the maximum dimension of the target in small cubes whose diagonal is equal to the resolution bin.
2. Form an accumulator array matching the quantization of the position space and set all elements to zero.

3. For each cube, we calculate the smallest distance form the cube to the 1-D scattering centers at all the sampling aspect angles (θ_n, γ_m), $n = 1, 2, \ldots, N$; $m = 1, 2, \ldots, M$:

$$d(n, m) = \min_i \left[x \cos \gamma_m \cos \theta_n + y \cos \gamma_m \sin \theta_n + z \sin \gamma_m - r_i(\theta_n, \gamma_m) \right] \quad i = 1, 2, \ldots, I \quad (3)$$

Then, for each sampling aspect (θ_n, γ_m), we compute whether the the following inequality is satisfied:

$$d(n, m) \leq \rho \tag{4}$$

where ρ is a parameter which is used to design the critical distance. Usually ρ approximates to a half of the range resolution, i.e., $\rho \approx c/(4B)$, B denotes the bandwidth. In other words, for each $d(n, m)$, if inequality (4) is satisfied, the corresponding accumulator cell is increased by one. After this step, all the cells in the accumulator array have a value in the zone $[0, MN]$.

4. After that, we sort all the accumulator cells in descending manner, and take 2000 cubes which correspond to the first 2000 cells as the candidate positions for 3D scattering centers.

By taking the steps above, the candidate positions for 3D scattering centers are available. However, most of the candidates are not the true positions for 3D scattering centers. Therefore, we will get rid of the false positions for 3D scattering centers in the next step.

3.1.2. Candidates Discriminating

This is a key step and we remove the false positions for 3D scattering centers by taking the following steps:

1. For each candidate, suppose the value of the corresponding cell is P. We first find the P corresponding 1-D projective positions from the estimated matrix $r_k(\theta_n, \gamma_m)$ that satisfy inequality (4) and treat them as a group. The 1-D projective positions and the corresponding aspects in the group are numbered as r_p and (θ_p, γ_p), respectively.

2. Divide the group into small groups, where each group contains only ten positions and the corresponding aspects. The residual part of the results can be neglected. It should be noted that smaller group may bring more errors, while bigger group means less new 3D positions. Therefore, we choose ten elements as a group to extract the new 3D positions.

3. We calculate a new 3D position for each small group by the linear least squares algorithm, which can be expressed as:

$$\mathbf{R} = [x_{new}, y_{new}, z_{new}]^T = \left(\mathbf{D}^H \mathbf{D} \right)^{-1} \mathbf{D}^H \mathbf{r} \tag{5}$$

$$\mathbf{D} = \begin{bmatrix} \cos \gamma_1 \cos \theta_1 & \cos \gamma_1 \sin \theta_1 & \sin \gamma_1 \\ \cos \gamma_2 \cos \theta_2 & \cos \gamma_2 \sin \theta_2 & \sin \gamma_2 \\ \ldots & \ldots & \ldots \\ \cos \gamma_{10} \cos \theta_{10} & \cos \gamma_{10} \sin \theta_{10} & \sin \gamma_{10} \end{bmatrix} \tag{6}$$

$$\mathbf{r} = \begin{bmatrix} r_1 & r_2 & \ldots & r_{10} \end{bmatrix}^T \tag{7}$$

where $\mathbf{R}$ represents the new 3D position calculated by (5). $\mathbf{r}$ and $\mathbf{D}$ represent the 1-D projective positions and unit vectors of corresponding aspects. The 3D positions can be viewed as the possible refinements of the candidate. If the candidate is a true position for 3D scattering centers, most of the new 3D positions will locate in a very small area. Otherwise, the new 3D positions will distribute in large space.

4. Repeat the above steps until all the candidates are processed. After that, we combine the close 3D positions by using a clustering algorithm, i.e., if the maximum distance of some 3D positions is smaller than a critical value, all this 3D positions are assumed to be produced by one scattering center whose position is the barycenter of the 3D positions. It should be noted that the more 3D positions a cluster contains, the more likely they are produced by a scattering center, and if a cluster contains few 3D positions, it is probably produced by an illusive scattering center. In this paper, all the clusters that contain more than twenty 3D positions are used to generate 3D positions for scattering centers, while the clusters that contain less than twenty 3D positions are treated as false positions and not considered in this paper.

5. After the number of scattering centers K and the 3D positions for every scattering center $\{x_k, y_k, z_k\}$ are estimated, the elements $a_{k,n,m}$ in $\mathbf{A}_k$ can be estimated by the linear least squares algorithm. The scattering coefficient not on the grids can be interpolated from nearby samples.

3.2. Analysis

3.2.1. Procedure Comparison

Figure 2 shows the procedure for 3D positions estimation of proposed method and the algorithm proposed in [9]. In [9], the OTSM map is used to calculate the values of the accumulator cells. Then the scattering centers' locations are obtained by seeking the cells with highest value one by one. The accumulator cells are renewed after taking each cell with highest value. Comparing with [9], the accumulator cells that maybe the positions of scattering centers are extracted once as candidates. Then the candidates are evaluated using (5) and refined by a clustering algorithm. The transform to the OTSM map is unnecessary in the proposed method, which is an advantage for realization. What is more, the clean step, which is time consuming, is not used in this paper. As a result, the computation complexity is greatly reduced in our proposed method.
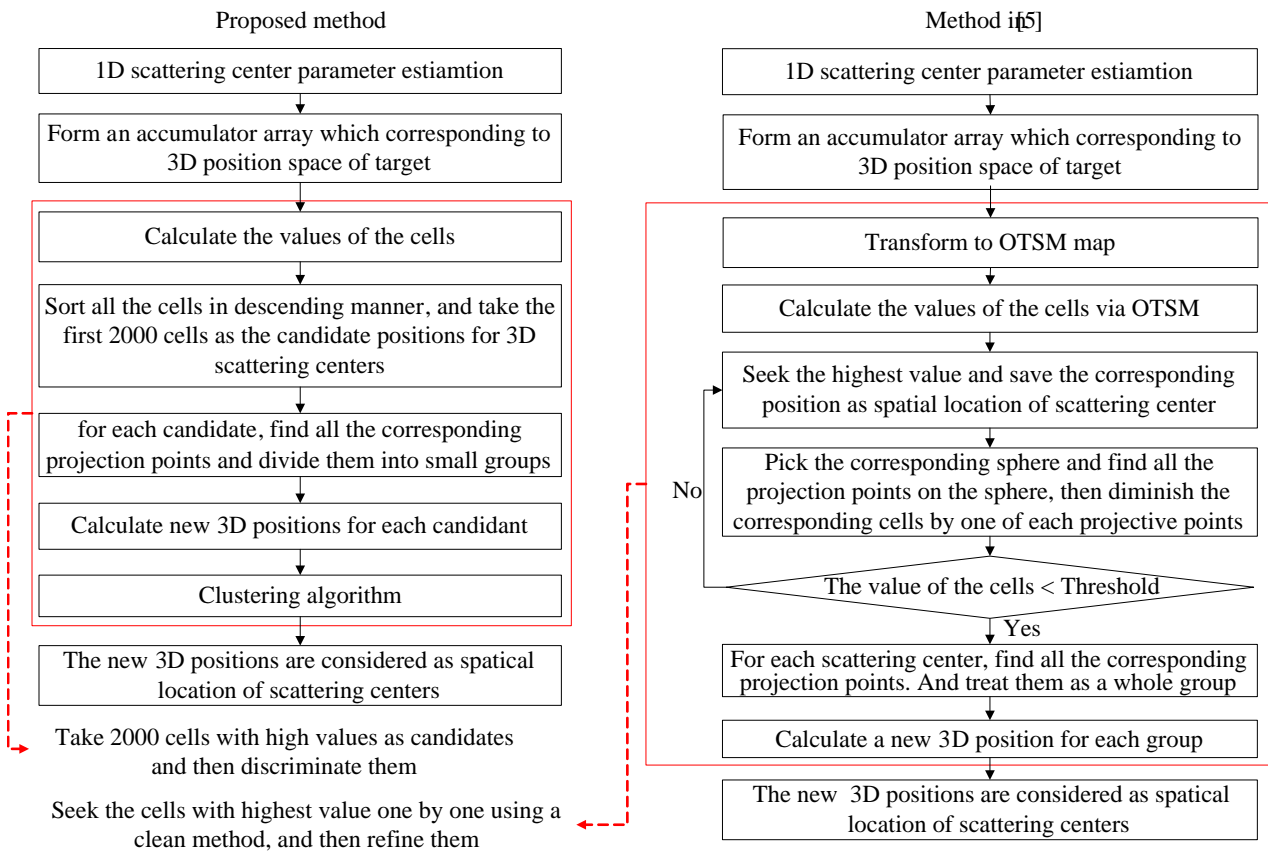
Figure 2. The procedure of 3D positions estimation for scattering centers.

3.2.2. Computational Cost

Assume that the position space can be divided into $O \times P \times Q$ tubes, where O, P, and Q represent the numbers of tubes in the x, y, and z dimensions, respectively. The sample numbers of the measurements in azimuth and elevation dimensions are N and M, respectively. There are five times of number multiplication and three times of number addition in (3) while (4) requires one time of number addition. Thus, Step 3 requires $5MNOPQ$ times of number multiplication and $4MNOPQ$ times of number

Table 1. The computational cost comparison.

Method	Computation cost	
	Times of number multiplication	**Times of number addition**
Proposed	$5MNOPQ + 2000A(16G + 45)/G$	$4MNOPQ + 2000A(12G + 28)/G$
HTBT	$5MNOPQ + 5OPQ + IMNPQ$	$4MNOPQ + IMNPQ$

addition. Suppose the average number of 1-D projective positions that corresponding to each scattering center is A and each group contains G elements. $\mathbf{D}$ is a $3 \times G$ matrix, and $(\mathbf{D}^H\mathbf{D})^{-1}$ needs $11G + 36$ times of number multiplication and $9G + 25$ times of number addition. Therefore, calculating (5) requires $16G + 45$ times of number multiplication and $12G + 28$ times of number addition. Generally, there are A/G groups for each scattering center. The computational cost is doubled 2000 times in the Step 4. Ignoring the low computational cost of other steps, the proposed algorithm proposed in this paper approximately requires $5MNOPQ + 2000A(16G + 45)/G$ times of number multiplication and $4MNOPQ + 2000A(12G + 28)/G$ times of number addition.

In [9], the transformation to OTSM map needs $5OPQ$ times of number multiplication. The computational cost of calculating the values of the cells is the same with the proposed method. However, for each repetition in the clean algorithm, $5MNPQ$ times of number multiplication and $MNPQ$ times of number addition are required, where P and Q should be large enough to ensure the effectiveness of the algorithm. The computational cost is doubled I times to extract all the I scattering centers. Therefore, it totally requires $5MNOPQ + 5OPQ + IMNPQ$ times of number multiplication and $4MNOPQ + IMNPQ$ times of number addition. This is why the authors claim that the computational cost and the requirement for storage are very high. We present the computational cost of these three methods in Table 1. Because A denotes the average number of 1-D projective positions corresponding to each scattering center, the following inequality holds: $A \ll MN$. Usually, there are hundreds of tubes in different dimensions. As a result, $2000A(16G + 45)/G \approx 32000A$ is much smaller than $IMNPQ$. It is noted that when the number of scattering center I increases, the complexity of HTBT increases. This indicates that when I is large, the proposed method is much more efficient than HTBT. It has been proven that considerable computational cost can be saved with our algorithm than Hough transform based technique (HTBT) in [9].

4. EXPERIMENTAL RESULTS

In this section, several examples are presented to demonstrate the effectiveness of the proposed procedure for scattering center extracting. First, example of scattering centers extracting of an aircraft carrier is presented, using the measured data obtained by a high frequency electro-magnetic simulation code. After that, we investigate the performance of the proposed procedure through another example of a tank.
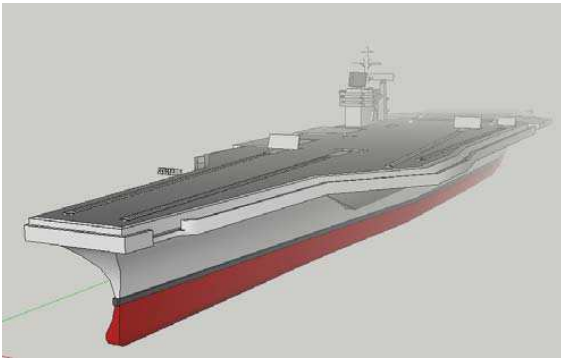
Figure 3. Geometry of the aircraft carrier.
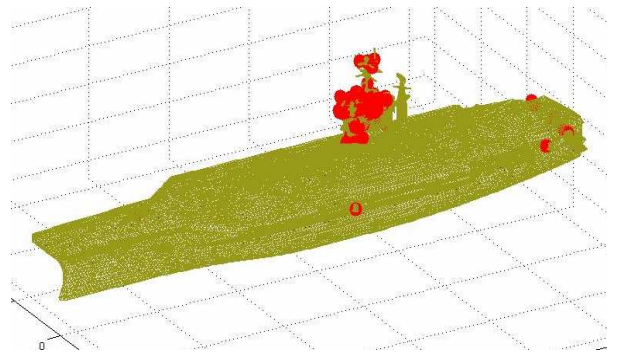
Figure 4. The position of the extracted scattering centers in the CAD model.

4.1. 3D Scattering Center Extracting of an Aircraft Carrier Model

In this experiment, we make use of an aircraft carrier model to validate the method. The geometry of the model is illustrated in Figure 3. The length, width, and height of the target are 320 m, 78 m, 75 m, respectively. The original data is produced by a high frequency electromagnetic simulation code. The frequency steps is from 16.975 GHz to 17.025 GHz with 151 sample points; The azimuth varies from 0°–360° with angle interval 1°; The elevation varies from 5°–85° with angle interval 5°.

Using the procedure proposed in this paper, a 3D scattering centers model which contains 50 scattering centers is obtained. In Figure 4, the scattering center model is positioned in the same Cartesian coordinates with the CAD model, from which we can see that the model is in accordance with the target structures and most of them located on the tips or edges on the target surface. In order to perform the effect of the proposed procedure, both the RCS data reconstructed by the extracted model and the RCS data of original measurements are investigated, as shown in Figure 5. The parameters used in calculating the simulated RCS data are supposed to be the same with original measurements. As shown in Figure 5, the RCS behaves approximately the same at different azimuth angles. This proves the effectiveness of the scattering center model in simulating the RCS data.

Figure 6(a) compares the original and reconstructed wide-band data. The azimuth angle and the elevation angle in Figure 6 are $\varphi = 1°$ and $\theta = 5°$, respectively. As we can see, the data behaves approximately the same at different frequencies; the range profiles of the original and reconstructed wide-band data are shown in Figure 6(b), where the location and the amplitude of the peaks in the original range profile can be retained in the reconstructed range profile. In order to evaluate the performance of the model in all aspects, the range profiles at all the azimuth angles are lined up and
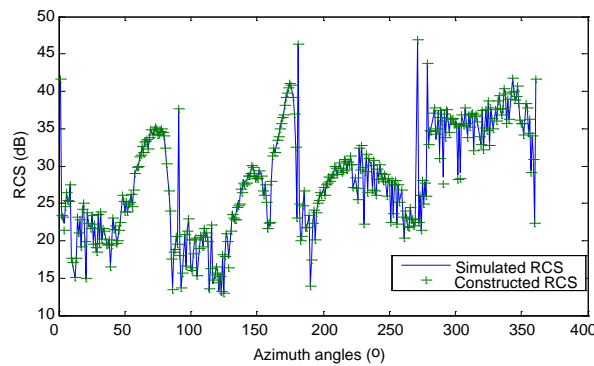
Figure 5. The RCS data reconstructed by the extracted model and the RCS data of original measurements.

(a)   (b)
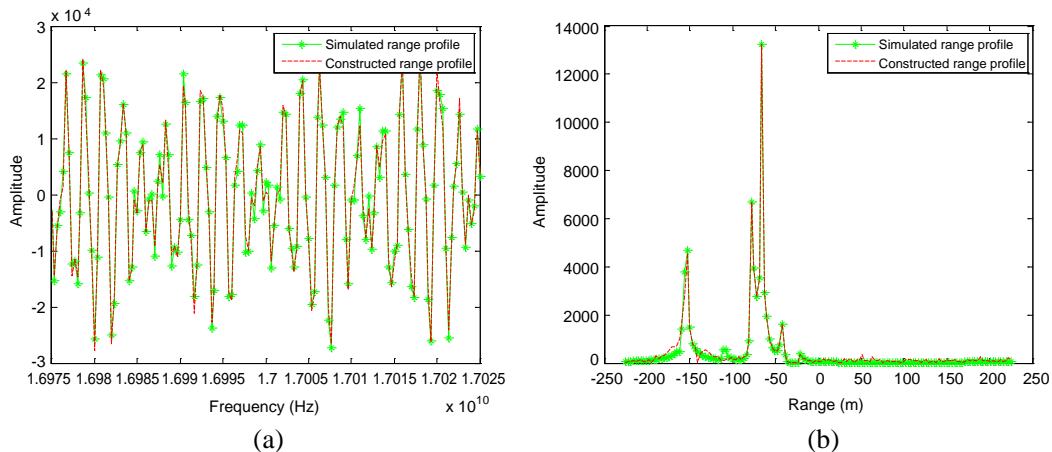
Figure 6. The wide-band RCS comparison between the original data and the reconstructed data. (a) Wide-band data comparison. (b) Range profile comparison.
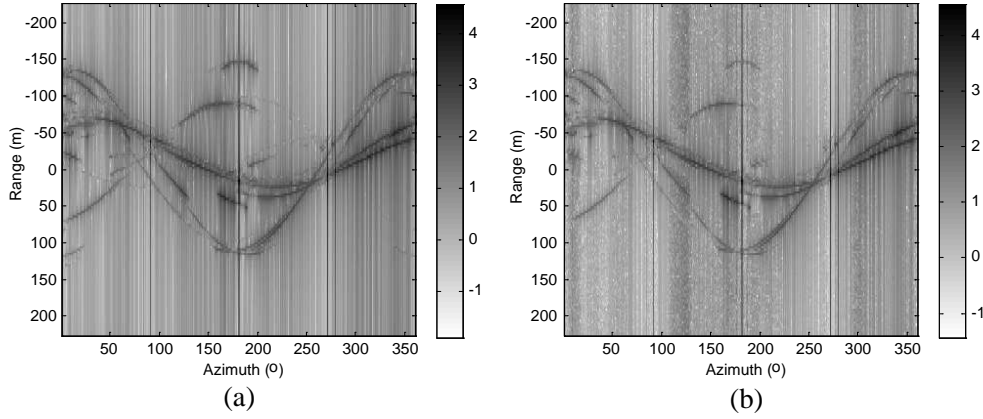
Figure 7. Comparison of range profiles at all azimuth angles. (a) Original data. (b) Reconstructed data.

the gray level of the pixels corresponds to the logarithm amplitude of the range profiles, as shown in Figure 7. One can see that a few dark curves crossing different angular extents in the original subfigure, which imply that the regular variation in projective location of the stable scattering centers. Comparing the results in Figure 7, we see that the intensity and location of the dominant scattering centers are retained in the reconstructed profiles at all azimuths. The results confirm the validity of the scattering center model.

In order to characterize the performance quantitatively, two kinds of matching correlation coefficients are considered between the original and reconstructed data here, i.e., the RCS correlation coefficients and the HRRP correlation coefficients. They can be defined as follows, respectively.

$$\text{Correlation}_{\text{RCS}} = \frac{1}{MN} \sum_{m=1}^{M} \sum_{n=1}^{N} \frac{\sum_{l=1}^{L} |rcs(l)rcs_{simu}(l)|^2}{\sqrt{\sum_{l=1}^{L} |rcs(l)|^2} \sqrt{\sum_{l=1}^{L} |rcs_{simu}(l)|^2}} \tag{8}$$

$$\text{Correlation}_{\text{HRRP}} = \frac{1}{MN} \sum_{m=1}^{M} \sum_{n=1}^{N} \frac{\sum_{s=1}^{S} |hrrp(s)hrrp_{simu}(s)|^2}{\sqrt{\sum_{s=1}^{S} |hrrp(s)|^2} \sqrt{\sum_{s=1}^{S} |hrrp_{simu}(s)|^2}} \tag{9}$$

where $rcs(l)$ denotes the original RCS measured at different frequency, $l = 1, 2, \ldots, L$ is the frequency-sampling points. $rcs_{simu}(l)$ is the reconstructed RCS. $hrrp(s)$ and $hrrp_{simu}(s)$ are the constructed range profile and original range profile, respectively. $s = 1, 2, \ldots, S$ is the index of the range bin. The correlation coefficients of different methods are listed in Table 2, which shows the proposed method performs better than HTBT. The reason is that HTBT extracts the scattering centers one by one. The computational complexity increases rapidly with the scattering center number. To insure HTBT effective and realizable, some scattering centers that exist in small aspect scope are not considered as global scattering centers, which may lead to some estimation errors. The proposed algorithm can extract a lot of candidates at once, and discriminate efficiently. Thus a more accurate model can be acquired.

4.2. 3D Scattering Center Extracting of a Heavy-Transport Truck

The above example demonstrates effectiveness of the proposed method applied in extracting the scattering centers from ship-shaped targets. However, different kinds of targets may have different electromagnetic characters. In the example, we evaluate our method using a car-shaped target. The

Table 2. Correlation coefficients of the two methods.

Correlation coefficients	HTBT	Proposed method
Correlation$_{\mathrm{RCS}}$	0.8276	0.9984
Correlation$_{\mathrm{HRRP}}$	0.8861	0.9714

Table 3. Correlation coefficients of the two methods.

Correlation coefficients	HTBT	Proposed method
Correlation$_{\mathrm{RCS}}$	0.7168	0.9975
Correlation$_{\mathrm{HRRP}}$	0.8935	0.9932

scattering data of a heavy model is measured by a high frequency electromagnetic simulation code. The frequency steps is from 16.75 GHz to 17.25 GHz with 101 sample points; the azimuth varies from 0°–360° with angle interval 1°; the elevation varies from 1°–70° with angle interval 1°. Figure 8 shows a picture of the target.

Figure 9 shows the positions of the 3D scattering centers model that extracted from the wideband measurements. Figure 10 and Figure 11 show the RCS data and range profiles generated by reconstructed data, from which we can see that the values are approximately the same to that obtained by measured data. The range profiles at all the azimuth angles are shown in Figure 12, and the correlation coefficients of different methods are summarized in Table 3. As one can see, the results demonstrate effectiveness of the scattering center model once more.
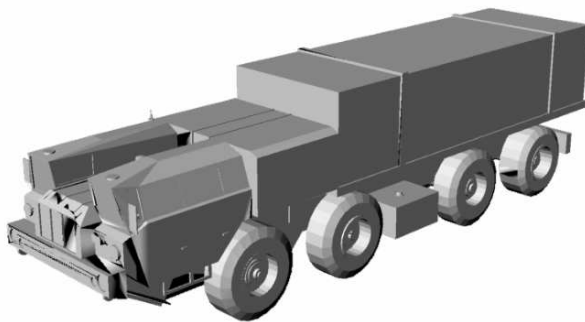
Figure 8. Picture of a heavy-transport truck.
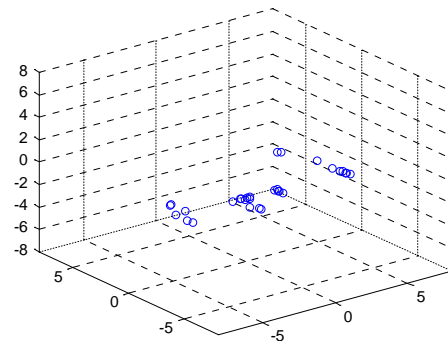
Figure 9. The position of the extracted scattering centers.
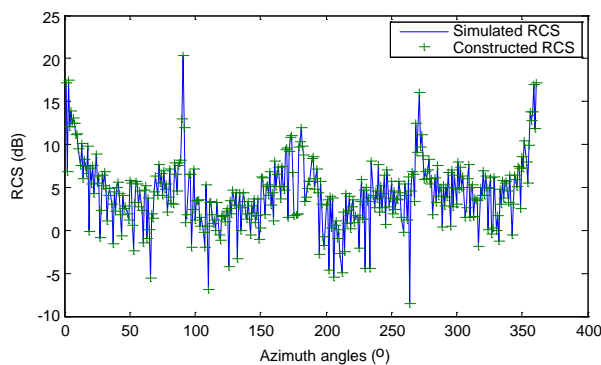
Figure 10. The RCS data reconstructed by the extracted model and the RCS data of original measurements.
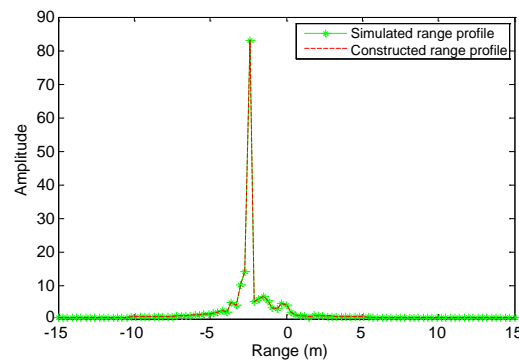
Figure 11. The Range profile comparison between the original data and the reconstructed data.
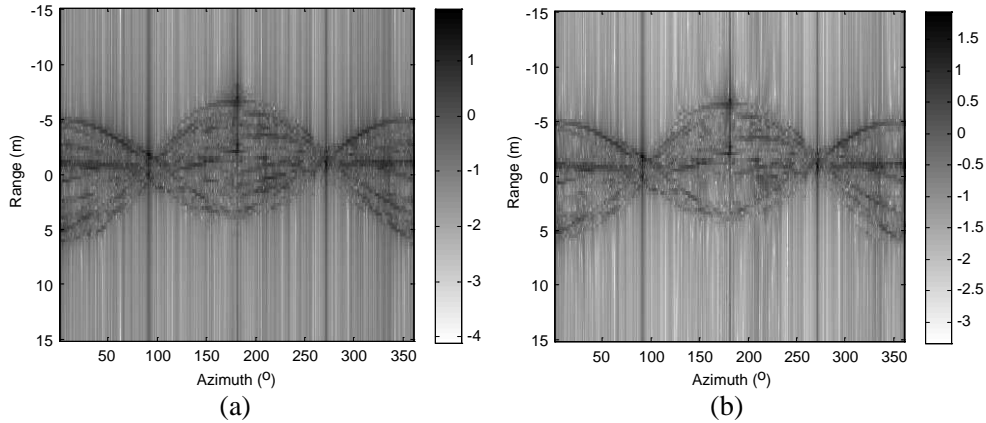
Figure 12. Comparison of range profiles at all azimuth angles. (a) Original data. (b) Reconstructed data.

5. CONCLUSIONS

The global 3D scattering center extraction is very useful for target recognition and data compression. However, the HTBT is inefficient for scattering centers model extraction because the scattering centers are extracted one by one. In this paper, a novel scattering center estimating approach has been developed for the global 3D scattering center extraction. In our approach, the candidate positions for 3D scattering centers are extracted by searching the estimated 1D scattering centers. After that, the scattering centers are obtained by evaluating the candidates. The approach is very efficient in time because the clean step is not required. Moreover, it is more effective than HTBT; the reason is that HTBT may discard some aspect-sensitive scattering centers. The experiment results demonstrate the performance of the proposed approach. It is believed that its efficiency in time and effectiveness make it useful in target recognition.

REFERENCES

1. Keller, J. B., "Geometrical theory of diffraction," *J. Opt. Soc. Amer.*, Vol. 52, No. 2, 116–130, Feb. 1962.
2. Potter, L. C., D. M. Chiang, R. Carriere, and M. J. Gerry, "A GTD-based parametric model for radar scattering," *IEEE Trans. Antennas Propag.*, Vol. 43, No. 10, 1058–1067, Oct. 1995.
3. Hurst, M. P. and R. Mittra, "Scattering center analysis via Prony's method," *IEEE Trans. Antennas Propag.*, Vol. 35, No. 8, 986–988, Aug. 1987.
4. Valagiannopoulos, C. A., "Arbitrary currents on circular cylinder with inhomogeneous cladding and RCS optimization," *Journal of Electromagnetic Waves and Applications*, Vol. 21, No. 5, 665–680, 2007.
5. Hoop, A. T., "Theorem on maximum absorption of electromagnetic radiation by a scattering object of bounded extend," *Radio Sci.*, Vol. 16, 971–974, 1981.
6. Swanson, N. L. and B. D. Billard, "Electively maximizing and minimizing the scattering and absorption of electromagnetic waves," US Patent 6842242 B2, 2005.

7. Valagiannopoulos, C. A., "On smoothening the singular field developed in the vicinity of metallic edges," *International Journal of Applied Electromagnetics and Mechanics*, Vol. 31, 67–77, 2009.

8. Bhalla, R., J. Moore, and H. Ling, "A global scattering center representation of complex targets using the shooting and bouncing ray technique," *IEEE Trans. Antennas Propag.*, Vol. 45, No. 12, 1850–1856, Dec. 1997.

9. Zhou, J., H. Zhao, Z. Shi, and Q. Fu, "Global scattering center model extraction of radar targets based on wideband measurements," *IEEE Trans. Antennas Propag.*, Vol. 56, No. 7, 2051–2060, Jul. 2008

10. McClure, M., R. C. Qiu, and L. Carin, "On the superresolution identification of observables from swept-frequency scattering data," *IEEE Trans. Antennas Propag.*, Vol. 45, No. 4, 631–641, Apr. 1997

11. Guo, K.-Y., Q.-F. Li, X.-Q. Sheng, and M. Gashinova, "Sliding scattering center model for extended streamlined targets," *Progress In Electromagnetics Research*, Vol. 139, 499–516, 2013.

12. Zhan, R. and J. Wan, "Iterated unscented Kalman filter for passive target tracking," *IEEE Transactions on Aerospace and Electronic Systems*, Vol. 43, No. 3, 1155–1162, 2007.

13. Zhan, R., Y. Gao, J. Hu, and J. Zhang, "SMC-PHD based multitarget track-before-detect with nonstandard point observations model," *Journal of Central South University*, 2014.

14. El Assad, S., X. Morin, and D. Barba, "Compression of polarimetric synthetic aperture radar data," *Progress In Electromagnetics Research*, Vol. 39, 125–145, 2003.

15. You, Y. N., H. P. Xu, C. S. Li, and L. Q. Zhang, "Data acquisition and processing of parallel frequency SAR based on compressive sensing," *Progress In Electromagnetics Research*, Vol. 133, 199–215, 2013.

16. Zhang, X., J. Qin, and G. Li, "SAR target classification using Bayesian compressive sensing with scattering centers features," *Progress In Electromagnetics Research*, Vol. 136, 385–407, 2013.

17. Makal, S., A. Kizilay, and L. Durak, "On the target classification through wavelet-compressed scattered ultrawide-band electric field data and ROC analysis," *Progress In Electromagnetics Research*, Vol. 82, 419–431, 2008.

18. Hu, J. M., W. Zhou, Y. W. Fu, X. Li, and N. Jing, "Uniform rotational motion compensation for ISAR based on phase cancellation," *IEEE Geosci. Remote Sensing Lett.*, Vol. 8, No. 4, 636–640, Jul. 2011.

19. Hu, J., J. Zhang, Q. Zhai, R. Zhan, and D. Lu, "ISAR imaging using a new stepped-frequency signal format," *IEEE Transactions on Geoscience Remote Sensing*, Vol. 52, No. 7, 4291–4305, Jul. 2014.

20. Huffel, S. V., H. Park, and J. B. Rosen, "Formulation and solution of structured total least norm problems for parameter estimation," *IEEE Transactions on Signal Processing*, Vol. 44, No. 10, 2464–2474, Oct. 1996.

21. Chen, F. J. and C. Carrson, "Estimation of two-dimensional frequencies using modified matrix pencil method," *IEEE Transactions on Signal Processing*, Vol. 55, No. 2, 718–724, Jan. 2007.

22. Schmidt, R. O., "Multiple emitter location and signal parameter estimation," *IEEE Trans. Antennas Propag.*, Vol. 34, No. 3, 276–280, Mar. 1986.

23. Roy, R. and T. Kailath, "ESPRIT-estimation of signal parameters via rotational invariance techniques," *IEEE Transactions on Acoustics, Speech and Signal Processing*, Vol. 37, No. 7, 984–995, Jul. 1989.

24. Yan, X., J.-M. Hu, G. Zhao, J. Zhang, and J. Wan, "A new parameter estimation method for GTD model based on modified compressed sensing," *Progress In Electromagnetics Research*, Vol. 141, 553–575, 2013.